PNAS
www.pnas.org

Supplementary Information for

A beta-barrel for oil transport through lipid membranes: dynamic NMR structures of AlkL

Tobias Schubeis[1], Tanguy Le Marchand[1], Csaba Daday[2] Wojciech Kopec[2], Kumar Tekwani Movellan[3], Jan Stanek[1]†, Tom S. Schwarzer[4], Kathrin Castiglione[4]‡, Bert L. de Groot[2], Guido Pintacuda[1]* & Loren B. Andreas[1,3]*

Loren B. Andreas
land@nmr.mpibpc.mpg.de

Guido Pintacuda
guido.pintacuda@ens-lyon.fr

This PDF file includes:

Other supplementary materials for this manuscript include the following:

One Supplementary Movie

Supplementary Text

Methods

Sample preparation. AlkL (28-230) from *Pseudomonas putida* GPo1 (Uniprot Q00595) with a C-terminal His-8 tag was expressed in *E. coli* as inclusion bodies, purified under denaturing conditions and refolded into LDAO micelles. A detailed protocol for AlkL refolding has been described previously(1) and was recently adapted to accommodate isotopic labelling(2). Isotopic labelling was performed in minimal media containing 4 g/L ^{13}C-glucose and 1 g/L $^{15}NH_4Cl$ (U-CN protein) or 4 g/L ^{13}C,^{2}H-glucose and 1 g/L $^{15}NH_4Cl$ in D_2O (U-DCN protein, 100% back exchange of NH-protons during purification). The detergent was exchanged to 2% octyl glucoside (OG) using a PD10 desalting column for solution NMR as well as for reconstitution into Lipids. The final solution NMR sample contained 330 µM U-DCN AlkL in 2 % OG and NMR buffer composed of 20 mM Sodium Phosphate at pH 7, with 10 mM glutamate, 10 mM arginine, and 0.02 % sodium azide. Traces of the refolding detergent LDAO may remain. To identify residues involved in hydrogen bonds, the buffer was exchanged to 20 mM Sodium Phosphate pH 7, 95% D_2O using a desalting column. In order to allow solution NMR analysis of AlkL in lipids, a nanodisc sample was prepared according to published protocols using membrane scaffold protein (MSP1D1)(3).

Lipid bilayer samples for solid-state NMR were prepared by addition of DMPC (10 mg/ml, multilamellar vesicles in H_2O) to AlkL in OG detergent at a lipid to protein ratio of 1:2 (w/w). Protein and lipids form soluble mixed micelles at this stage. Detergent was subsequently removed by dialysis against NMR buffer resulting in formation of multilamellar vesicles that precipitate within 24 hours. The white precipitate was collected by centrifugation using a table top centrifuge, resuspended in 0.5 ml buffer and packed into 1.3 or 0.7 mm rotors (Bruker) using an ultracentrifuge packing device (Giotto Biotech). To investigate the effect of the presence of a hydrophobic small molecule, a solid-state NMR sample was equilibrated with buffer saturated with carvone or octane and compared with a second rotor packed from the same batch of precipitated protein.

The bilayer sample in LPS (Sigma, phenol extract purified from *E. Coli* K-235) were prepared in an identical manner, except that the reconstitution was performed from AlkL in OG detergent with a ratio of DMPC:LPS:AlkL of 1:1:2 (by weight). The pellet was nearly transparent, different from the white precipitate that forms in the presence of DMPC alone. The spectrum (Fig S5) is nearly unchanged as compared to the DMPC preparation.

Solution NMR Spectroscopy. Triple resonance solution NMR spectra were recorded on a 600 MHz Bruker Avance III instrument equipped with a cryogenic probe. TROSY based HSQC, HNCA, HN(CO)CA, HNCACB, HNCO, and HN(CA)CO spectra were used for resonance assignment(4). To obtain distance restraints, a 3D NOESY-^{15}N-TROSY (NHH) and a 3D ^{15}N-HSQC- NOESY-^{15}N-HSQC (NNH) was recorded on a 1000 MHz Bruker Avance III instrument equipped with a cryogenic probe. All spectra were recorded at a sample temperature of 308 K.

Solid state NMR Spectroscopy. NMR spectra for the assignment of backbone and sidechain resonances were (H)NH, (H)CH, (H)CANH, (H)(CO)CA(CO)NH, (H)CONH, (HCA)CB(CA)NH, (HCA)CB (CACO)NH, (H)NCAHA, (H)N(CO)CAHA, (H)CCH, (H)COCAHA, (H)CO(N)CAHA. These spectra were recorded on U-CN AlkL in a 0.7 mm MAS rotor at 111 kHz on a 1000 MHz Bruker Avance III spectrometer (5, 6). Additionally, we recorded spectra for assignments, (H)CANH, (HCO)CA(CO)NH, (H)CONH, (H)CO(CA)NH, (HCA)CB(CA)NH, on U-DCN AlkL in a 1.3 mm MAS rotor at 60 kHz on a 800 MHz Bruker Avance III spectrometer. To obtain distance restraints, we recorded H(H)NH and H(H)CH using RFDR, H(H)NH, (H)N(HH)NH and (H)C(HH)CH using BASS-SD on U-CN AlkL as well as a 4D (H)NH(H)NH using RFRD on U-DCN AlkL(2, 7). Further experimental details are tabulated in Extended Data Table 1. Relaxation rates (^{15}N R_1 and $R_{1\rho}$) were determined using a modified 3D (H)CONH experiment (pseudo-4D), with the longest relaxation delay at 54 seconds for R_1 and 200 ms for $R_{1\rho}$. Chemical shift perturbations induced by the presence of either octane or carvone were measured under saturating concentrations of the small molecule, and were evaluated as a combination of ^{1}H, ^{15}N and ^{13}CA shift changes, with relative scaling of 1, 0.15, and 0.3: $CSP = \sqrt{\frac{1}{3}(\partial\Delta_H{}^2 + 0.15\partial\Delta_N{}^2 + 0.3\partial\Delta_{CA}{}^2)}$. All spectra were recorded at a sample temperature of 305 ± 3 K.

Table S1. NMR parameters for RFDR and BASS-SD spectra.

Experiment	H(H)NH	H(H)NH	(H)N(HH)NH	H(H)CH	(H)C(HH)CH	(H)NH(H)NH	(H)NH(H)NH
Sample	$^{13}C,^{15}N$	$^{13}C,^{15}N$	$^{13}C,^{15}N$	$^{13}C,^{15}N$	$^{13}C,^{15}N$	$^{2}H,^{13}C,^{15}N$	$^{2}H,^{13}C,^{15}N$
Spectrometer (MHz)	1000	1000	1000	1000	1000	1000	800
MAS, ν_r (kHz)	111	111	111	111	111	60	60
Heteronuclear transfer 1	H-N CP	H-N CP	H-N CP	H-C CP	H-C CP	H-N CP	H-N CP
Field (kHz)	1.4/0.4 ν_r	1.4/0.4 ν_r	1.4/0.4 ν_r	1.4/0.4 ν_r	1.4/0.4 ν_r	1.6/0.6 ν_r	1.7/0.7ν_r
Time (ms)*	1	0.6	0.6	0.5	0.35	1	1
Heteronuclear transfer 2	N-H CP	N-H CP	N-H CP	C-H CP	C-H CP	N-H CP	N-H CP
Field (kHz)	0.4/1.4 ν_r	0.4/1.4 ν_r	0.4/1.4 ν_r	0.4/1.4 ν_r	0.4/1.4 ν_r	0.6/1.6 ν_r	0.7/1.7ν_r
Time (ms)*	0.4	0.3	0.3	200	0.19	0.6	0.6
H-H Transfer	RFDR	BASS-SD	BASS-SD	RFDR	BASS-SD	RFDR	RFDR
Field (kHz)	192	6.25	6.25	192	4.1	100	100
Time (ms)*	0.5	6	6	0.5	4.5	3	0.5
Heteronuclear transfer 3	–	–	H-N CP	–	H-C CP	H-N CP	H-N CP
Field (kHz)	–	–	1.4/0.4 ν_r	–	1.4/0.4 ν_r	1.6/0.6 ν_r	1.7/0.7ν_r
Time (ms)*	–	–	0.6	–	0.35	1	1
Heteronuclear transfer 4	–	–	N-H CP	–	C-H CP	N-H CP	N-H CP
Field (kHz)	–	–	0.4/1.4 ν_r	–	0.4/1.4 ν_r	0.6/1.6 ν_r	0.7/1.7ν_r
Time (ms)*	–	–	0.3	–	0.19	0.6	0.6
sw (t1) (ppm)	12.5	35	35	12.5	38	6.5	7
Acq.time (t1) (ms)	4.6	9	9	4.6	7.7	4.4	2.2
sw (t2) (ppm)	66	5.5	35	66	38	40	35
Acq.time (t2) (ms)	16.4	3.8	9	6.6	8.7	9.1	9.1
sw (t3) (ppm)	100	100	100	100	100	40	35
Acq.time (t3) (ms)	8	8	8	8	8	9.1	8.8
sw (t4) (ppm)	–	–	-	–	-	100	30
Acq.time (t5) (ms)	–	–	-	–	-	8	8
^{1}H decoupling	swTPPM	swTPPM	swTPPM	swTPPM	swTPPM	waltz	swTPPM
Field (kHz)	26	26	26	26	26	7.2	13
Interscan delay (s)	1	0.8	0.8	1	0.8	1.25	1
Number of scans	8	80	240	8	16	48	16
NUS (%)	–	–	–	–	–	2	–
Measurement time (d)	3	2.4	11.5	3	4.6	5.5	13

Resonance Assignment. We used FLYA(8) (34) with peak lists generated from spectra of the fully-protonated sample automatically in Sparky(9) or CCPN (10)(36). The threshold for peak identification was initially set such that only an estimated 5-10 false peaks were present (as determined by the number of peaks picked with incorrect sign). Subsequently, overlapping peaks and weaker peaks (that were not initially picked) were manually identified to extend the assignment. The automated assignments were verified and additional assignments completed manually.

Structure Calculation. Several unambiguous distance restraints were manually assigned in the well resolved 3D (H)N(HH)NH spectrum for the solution sample. Similarly, the 4D (H)NH(H)NH spectrum was used to identify unambiguous restraints in the lipid bilayer sample. We additionally used the chemical shifts to generate dihedral angle restraints using TALOS-N(11). These initial unambiguous restraints and dihedral angles clearly defined the β-barrel region, and additional structure in the loops for the lipid bilayer preparation. For the solution structure, an initial set of hydrogen bond restraints was defined for resonances that showed no exchange in D_2O. For both structures, hydrogen bond restraints were included where cross-peaks in the 4D spectrum were identified (Fig S3-4), and where chemical shifts were consistent with an extended conformation, as indicated in Fig. S9. A short stretch of helical hydrogen bonds in loop 2 was introduced for the bilayer structure, where chemical shifts indicated, and where an initial model showed a helical structure (Fig. S9). NOESY peak lists (solution) or RFDR and BASS-SD peak lists (solids) were added for automated assignment and structure calculation using CYANA 3.98 (12). Final numbers are listed in Extended Data Table 2. Figures were prepared with UCSF Chimera (13).

Table S2: Structure calculation statistics. Summary of identified cross-peaks and conformational restraints used in the structure calculation, and structure quality in terms of RMSD within a bundle of 20 conformers used to represent the ensemble.

Distance restraints	Lipids (MAS)	Detergents (solution)
Total	769	112
Short-range (|i-j|<=1)	425	53
Medium-range (1<|i-j|<5)	21	3
Long-range (|i-j|>=5)	323	56
h-bonds (manual restraints)	94	64
Dihedral angle restraints	303	206
Restraints per residue ˜	3.1 (3.7*)	1.3 (2.8#)
Backbone RMSD (Å)	0.66*	0.73#
Heavy atom RMSD (Å)	1.40*	1.52#

*calculated over structured regions, residues 12-33, 44-108, 116-156, 161-205 (22+65+41+45=173 residues)
˜excluding short-range restraints, excluding H-bond restraints to avoid overcounting.
#calculated over structured regions, residues 13-27, 52-74, 100-107, 116-126, 146-169 ,193-205 (15+23+8+11+24+13=94 residues)

Table S3. Residue specific chemical shift perturbation (CSP) and amide ^{15}N relaxation.

Residue	Octane CSP (ppm)	Carvone CSP (ppm)	Apo ^{15}N R_1 (s^{-1})	Apo ^{15}N $R_{1\rho}$ (s^{-1})
12	0.050	0.024		
13	0.094	0.034		18.6 ±0.01
14	0.022	0.033	0.047 ±0.004	12.0 ±0.06
15	0.026	0.030		
16	0.035	0.036		
17	0.049	0.031		
18	0.034	0.082		
19	0.063	0.026	0.019 ±0.005	7.7 ±0.12

20	0.035	0.039		9.2 ±0.11
21	0.167	0.069		8.6 ±0.09
22	0.057	0.056	0.014 ±0.003	10.4 ±0.10
23	0.050	0.111	0.024 ±0.005	
–				
25	0.159	0.062		
26	0.268			
27	0.080			
28	0.078			
29				
30	0.097			
31	0.042	0.044	0.093 ±0.045	17.7 ±0.26
32	0.332		0.040 ±0.013	22.8 ±0.57
33	0.047			11.7 ±0.21
34	0.054			
–				
39	0.024			
40	0.142			
41	0.073			
–				
45		0.113		
46	0.018	0.032		14.3 ±0.16
47	0.030	0.036		
48	0.283	0.107		
49			0.043 ±0.010	16.3 ±0.21
–				
54	0.026	0.067		
55	0.072	0.094		16.3 ±0.30
56	0.091	0.113	0.019 ±0.003	
57	0.147	0.082	0.024 ±0.006	9.4 ±0.11
58	0.133	0.096		
59	0.098	0.049	0.015 ±0.002	
60	0.055	0.035	0.014 ±0.004	10.3 ±0.13
61	0.055	0.018		5.9 ±0.06
62	0.020	0.033	0.013 ±0.003	7.8 ±0.06
63	0.046	0.051	0.025 ±0.006	15.0 ±0.25
64	0.032	0.053		
65	0.034	0.045		
66	0.027	0.040		108.4 ±3.8
67	0.024	0.010		11.5 ±0.09
68	0.030	0.032	0.013 ±0.002	7.7 ±0.04
69	0.020	0.025	0.012 ±0.002	5.8 ±0.03
70	0.035	0.023	0.014 ±0.002	7.3 ±0.04
71	0.066	0.031		
72	0.119	0.090	0.010 ±0.003	8.0 ±0.06
73	0.045			
–				
75			0.028 ±0.009	12.0 ±0.14
–				
77	0.365	0.188		28.0 ±0.67
78	0.121			
79	0.168	0.372	0.040 ±0.009	14.6 ±0.18
80	0.101	0.230		
81	0.169	0.025		13.2 ±0.18
82	0.154	0.166		

83	0.084	0.049	0.023 ±0.004	
84	0.054	0.018		12.4 ±0.07
85	0.029	0.041	0.037 ±0.004	12.8 ±0.08
86	0.099	0.062		
87	0.060	0.039		
88	0.150	0.049	0.091 ±0.029	13.4 ±0.21
89	0.087	0.055	0.040 ±0.010	13.5 ±0.16
90	0.124	0.068		
91	0.082	0.071	0.074 ±0.011	11.6 ±0.09
92	0.028	0.038	0.052 ±0.005	10.9 ±0.06
93	0.047	0.041	0.029 ±0.005	7.8 ±0.08
94	0.026	0.059	0.017 ±0.002	6.4 ±0.04
95	0.060	0.043		
96	0.094	0.099		9.5 ±0.07
97				12.6 ±0.26
–				
99	0.339	0.066	0.047 ±0.013	14.0 ±0.27
–				
101			0.029 ±0.008	
102	0.091	0.099	0.014 ±0.004	7.9 ±0.07
103	0.087	0.068	0.008 ±0.002	5.5 ±0.04
104	0.030	0.020	0.014 ±0.002	10.1 ±0.06
105	0.026	0.044	0.013 ±0.002	
106	0.056	0.057		
107	0.027	0.042	0.010 ±0.002	6.2 ±0.04
108	0.004	0.044		
109	0.123	0.078	0.006 ±0.002	9.6 ±0.07
110		0.041		
–				
115	0.148			
116	0.062			
–				
118	0.077	0.011		
119	0.036	0.029		
120	0.059	0.027	0.019 ±0.003	9.6 ±0.08
121	0.015	0.022	0.013 ±0.004	9.0 ±0.08
122	0.030	0.055		
123	0.044	0.045	0.018 ±0.004	5.7 ±0.05
124	0.101	0.123	0.018 ±0.004	10.8 ±0.11
125	0.129	0.087		9.9 ±0.12
126	0.337	0.170		
127	0.256	0.176	0.016 ±0.007	
128	0.022			
129	0.021			
130	0.031	0.051	0.034 ±0.006	
131	0.066	0.135		
132	0.082	0.072	0.028 ±0.004	7.7 ±0.08
133	0.014	0.022		
134	0.029	0.054	0.030 ±0.005	11.4 ±0.08
135	0.135	0.046	0.030 ±0.006	6.6 ±0.07
136	0.046	0.051		
137	0.067	0.037		
138	0.052	0.035	0.016 ±0.003	15.2 ±0.12
139	0.028	0.017		15.5 ±0.10
140	0.029	0.015		

141	0.097	0.063		6.0 ±0.06
142	0.223	0.206	0.041 ±0.009	8.7 ±0.01
143	0.028	0.022	0.045 ±0.005	7.7 ±0.04
144	0.133	0.050		9.4 ±0.12
145	0.133	0.104		9.3 ±0.21
146	0.064	0.111		9.8 ±0.12
–				
148	0.057	0.017		8.3 ±0.06
149	0.044	0.065		
150	0.043	0.030	0.009 ±0.002	9.1 ±0.05
151	0.012	0.031	0.011 ±0.002	7.9 ±0.04
152	0.035	0.060		
153	0.022	0.043	0.022 ±0.003	7.7 ±0.05
154	0.031	0.051		
155	0.022	0.024		
156	0.054	0.040		
157	0.049			
158	0.033			
–				
161	0.176	0.102		
162	0.012	0.033	0.025 ±0.008	10.4 ±0.11
163	0.031	0.034		
164	0.026	0.027		
165	0.035	0.040	0.029 ±0.003	6.6 ±0.04
166	0.048	0.028	0.027 ±0.006	9.3 ±0.09
167	0.069	0.071	0.014 ±0.002	7.1 ±0.04
168	0.069	0.115		
169	0.107	0.070		
–				
172	0.348	0.283		
173	0.264	0.204		
174	0.034		0.053 ±0.007	10.5 ±0.01
175	0.144	0.055	0.090 ±0.015	8.9 ±0.07
176	0.057	0.017		
177	0.039	0.033		
178	0.019	0.032	0.018 ±0.002	6.8 ±0.04
179	0.065	0.034	0.026 ±0.003	8.0 ±0.05
180	0.212	0.042		
181	0.182	0.035		
–				
183	0.003	0.017		
–				
185	0.044	0.020		
186	0.086	0.027		
187	0.205	0.105	0.040 ±0.009	11.1 ±0.15
188	0.112	0.066		13.0 ±0.18
189	0.057	0.053		
190	0.053	0.022		
191	0.156			14.7 ±0.17
–				
194	0.352			
195	0.224	0.123		
196	0.033	0.008	0.014 ±0.002	6.1 ±0.06
197	0.152	0.129	0.021 ±0.005	11.0 ±0.23
198	0.031	0.055		

199	0.031	0.019	0.010 ±0.003	9.0 ±0.07
200	0.070	0.037	0.016 ±0.004	7.2 ±0.07
201	0.059	0.028	0.016 ±0.005	8.3 ±0.09
202	0.041	0.066	0.019 ±0.004	9.6 ±0.09
203	0.045			
204	0.098			

***Relaxation data fitting*.** Signal intensity decays of both ^{15}N R_1 and $R_{1\rho}$ relaxation experiments were fitted to a monoexponential function. Error estimate was performed with Monte Carlo simulations: synthetic datasets are produced by adding Gaussian random noise (with same standard deviation as the experimental noise) to the back-calculated decay curves. The error was determined as the standard deviation of the ensemble of dynamical parameters obtained by fitting 1000 synthetic datasets.

MD Simulations: System preparation - AlkL NMR structure. The NMR structure of AlkL was aligned along the membrane normal using the Orientations of Proteins in Membranes (OPM) database(14) and subsequently embedded in a DMPC or LPS membrane and solvated with water molecules and 150 mM KCl using the CHARMM-GUI webserver (15). The full system contained ~160 000 atoms. The titratable groups of the protein were protonated according to their standard protonation states at pH 7, with an exception of D58, which was protonated, based on the spatial proximity of another negatively charged residue, D70 and robust binding of K^+ ion to (charged) D58 in initial simulations. Further, pKa values predicted by PROPKA(16) suggested that one of these aspartates (D58 or D70) should be in its protonated form.
The initial, multi-step equilibration of the system, with a gradual release of restrains acting on protein atoms, was conducted using scripts provided by CHARMM-GUI. Subsequently, the system was equilibrated for 100 ns, without any restraints, prior to production runs.
To study interactions and possible permeation of hydrophobic molecules through AlkL, 64 carvone molecules were placed in the aqueous phase of the last snapshot from the equilibration run.

***MD Simulations: System preparation - AlkL homology models*.** Two homology models of AlkL were built, using structures of OmpW and OprG proteins (PDB id: 2F1T and 2X27, respectively) as templates using the Swiss-model web server (swissmodel.expasy.org). Both homology models were then prepared for MD simulations in the same manner as the NMR structure.

***MD Simulation details*.** All simulations were performed with GROMACS 2018 simulation software(17). The CHARMM36m force field was used in all simulations (18). Lipids were modeled using the CHARMM36 force field (19). The *P. Aruginosa* LPS was chosen with Lipid A type 1, core 2, and 2x the standard O-antigen in the CHARMM gui (www.charmm-gui.org) with calcium counterions. The parameters for carvone were obtained from the CHARMM General Force Field (CGenFF) (20) webserver (https://cgenff.paramchem.org). Water was modeled using the CHARMM version of the TIP3P model(21), with LJ interactions placed on hydrogen atoms. Standard CHARMM parameters were used for K^+, Ca^{2+} and Cl^- ions (22). All bonds were constrained using LINCS, allowing for a 2fs time step (23). Non-bonded (van der Waals) interactions were force-switched off from 0.8 to 1.2 nm. Long-range electrostatic interactions were treated with PME with a 1.2 nm real space cutoff (24). The simulated systems were kept at a temperature of 320K and a pressure of 1 bar, using a Nosé-Hoover thermostat (25, 26) and a Parrinello-Rahman barostat(27), respectively.
For LPS simulations (Fig. S6), an initial simulation was carried out for 100 ns and 10 equidistant frames from this trajectory were extracted. Into each of these 10 frames, 100 randomly placed octanes were inserted, replacing about 1000 water molecules. Each of these 10 octane-containing frames were independently equilibrated 10 times and the 100 simulations were run for a total of ~15 μs. The top 10 trajectories (defined by the octane with the most contacts with AlkL and manually verified to be close to the exit site) out of these initial 100 were chosen and another 10 replicas from each were spawned and run for a total of ~50 μs.
The simplified DMPC-octane simulations were run in the presence of 64 randomly placed octanes in 11 independent simulations for a total of ~9 μs (Fig. S6).
Four systems containing AlkL in DMPC were simulated for 1000 ns each ('Alk apo' simulations). After the addition of carvone, four new systems were initially simulated for 1000 ns each. Further simulations were spawned by monitoring the position of bound carvone and simulated for additional 100 ns in several cycles, as shown in Fig. S7.

Systems containing homology models of AlkL were simulated with and without carvone for 1000 ns in 4 copies each. The total simulation time of all systems was ~34 μs and for the entire study, about 108 μs.

MD Simulation analysis. Exit pathways were identified and analysed using the MOLE 2.0 software(28) and CONAN (29). Remaining analysis was performed using GROMACS tools: cluster, covar, anaeig, distance and in-house written scripts. Molecular structures were rendered using VMD (30). Plots were made using NumPy and Matplotlib.

Supporting Figures

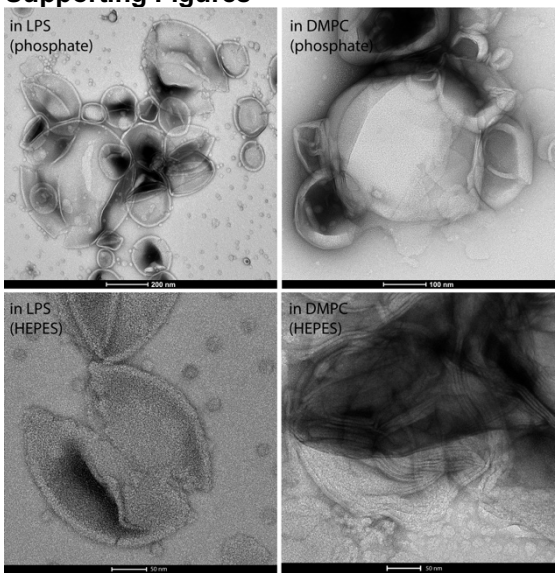

Figure S1. Negative stain EM images of the preparations used for NMR. Liposomes are observed. No protein aggregate was identified, and no evidence for ordered 2D crystalline arrays could be found.

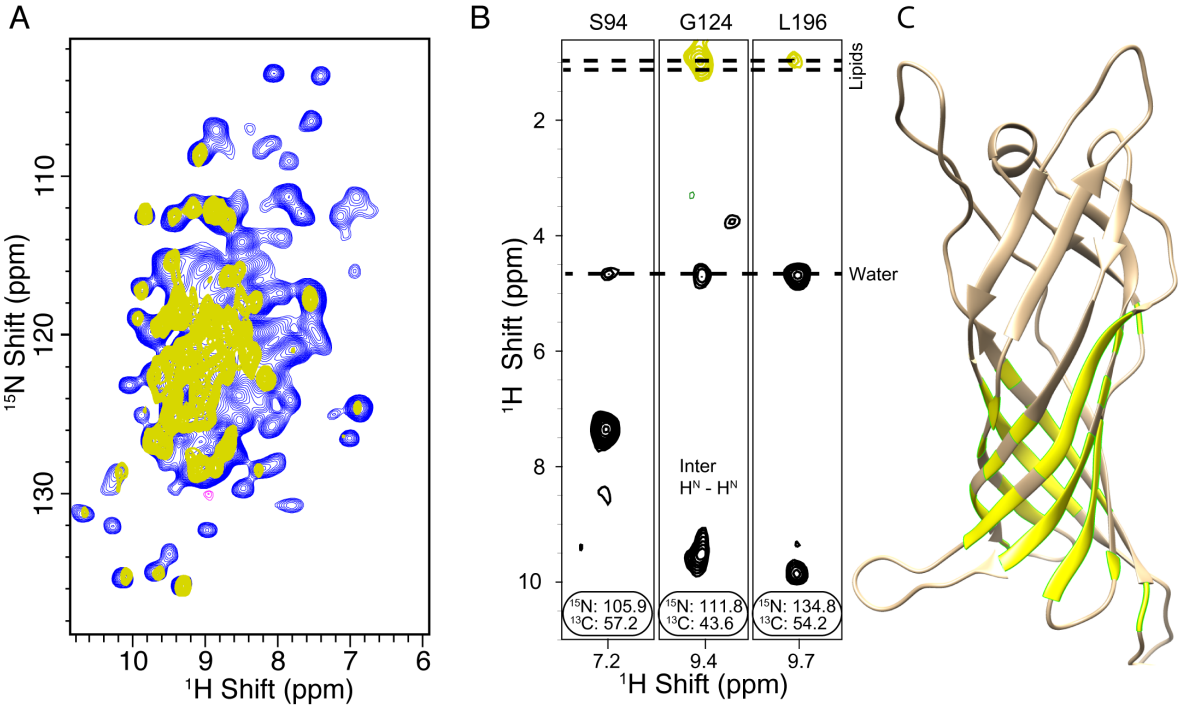

Figure S2. Lipid to protein magnetization transfer shows the lipid-embedded protein surface. In (A), the lipid plane of a 3D HhNH spectrum at about 1.1 ppm is colored in yellow. In (B) selected strips from a similar 4D spectrum, HhnCANH resolves resonance overlap in the 3D spectrum. 50 ms of Nuclear Overhauser Effect (NOE) mixing was used. In C, the residues for which lipid contacts are observed are colored in yellow on the solid-state NMR structure. Spectra were acquired at a 800 MHz spectrometer with 55 kHz MAS. The protein was deuterated to suppress any protein signals arising at the proton frequency of the lipid acyl chains.

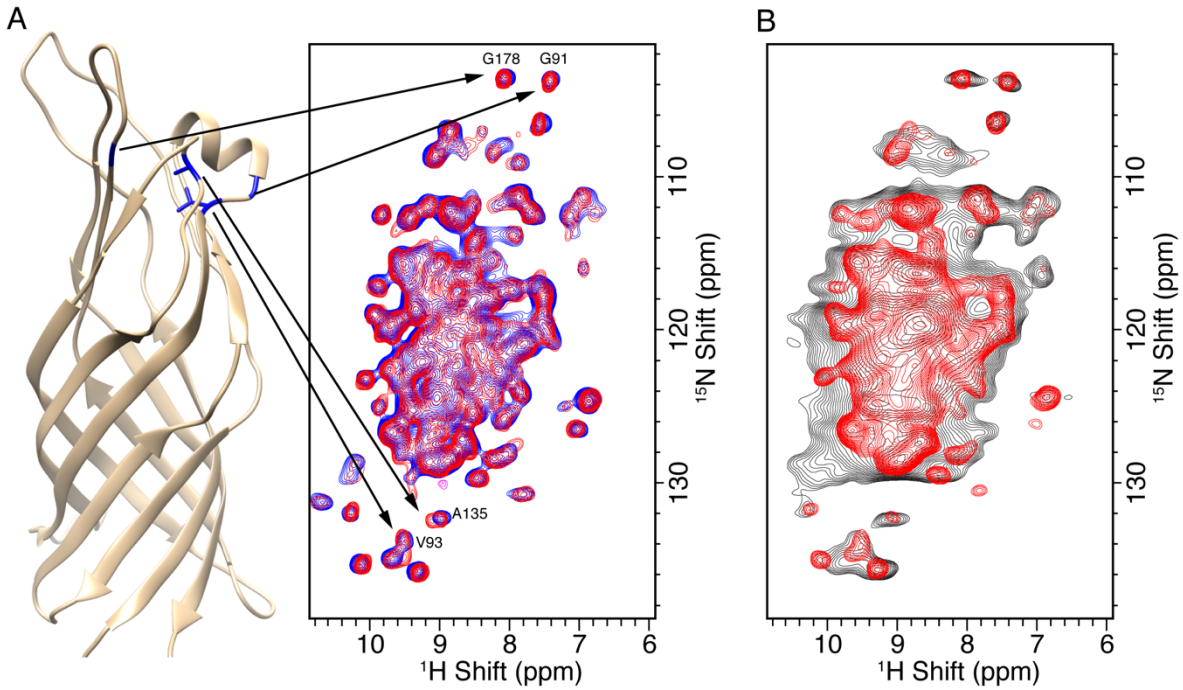

Figure S3. Spectra at varying DMPC lipid concentration. In (A), the a lipid protein ratio (LPR) of 10 (blue) is compared with a LPR of 0.5 (red). The spectra are nearly identical, and notably, several well-resolved resonances from the loops are unchanged in the dilute sample. In (B), degradation of the spectral quality is observed for an over concentrated sample with LPR of 0.25 (black) compared with a sample at 0.5 LPR (red). All spectra were recorded on a 700 MHz spectrometer with a spinning frequency of 60 kHz. Spectra in (A) were recorded with deuterated protein, and those in (B) with protonated protein.

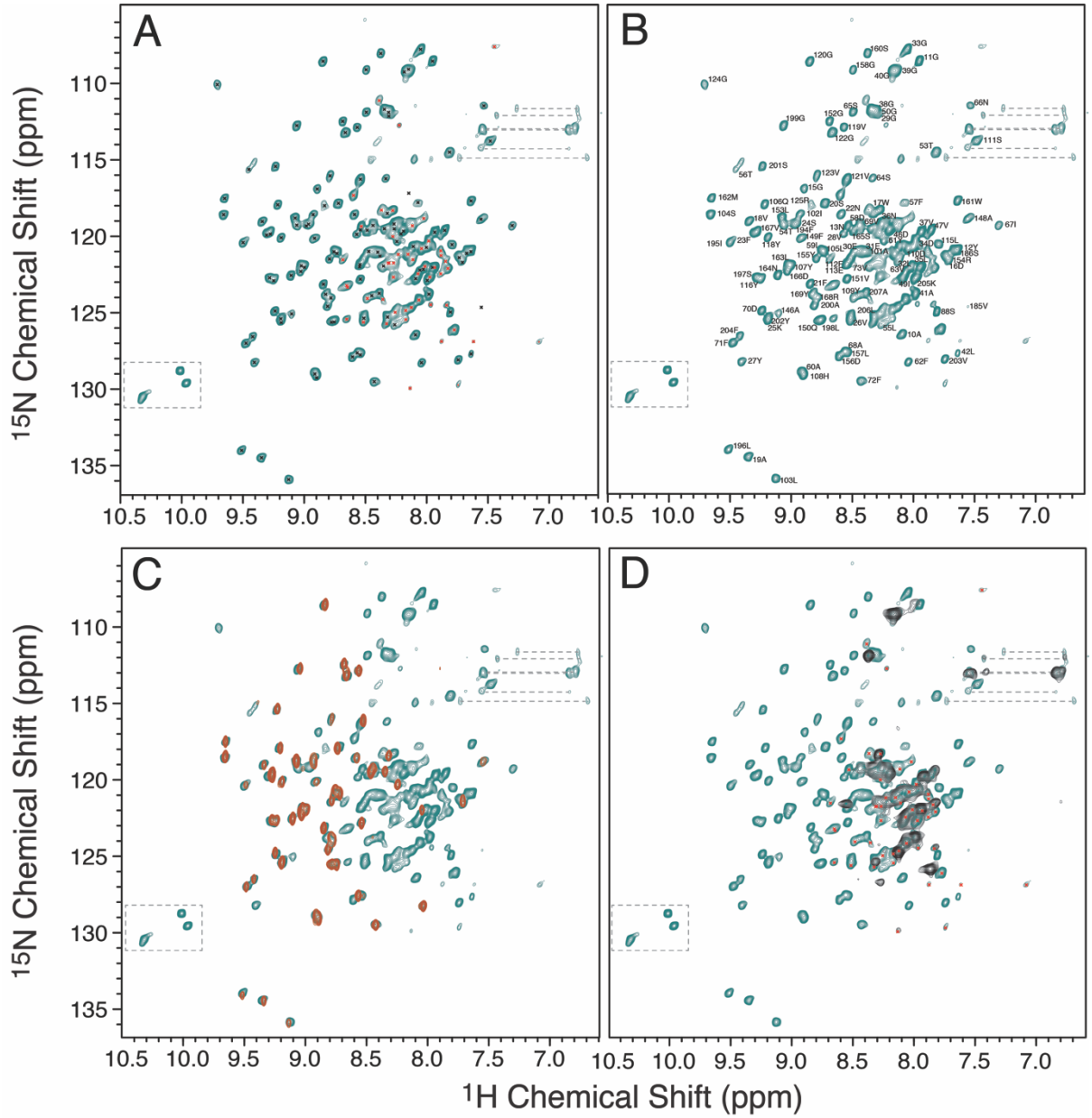

Figure S4. Solution ^{15}N-TROSY spectra of AlkL. In (A and D), unassigned resonances are indicated with red crosses. In (B), assignments are annotated. In (C), the red spectrum was recorded after 24 hours in D_2O, indicating exceptionally stable hydrogen bonds, which were used in the structure calculation. In (D), the black spectrum was recorded on AlkL in MSP1D1 DMPC nanodiscs. Only signals arising from highly flexible loops are detected, prohibiting structural analysis under these conditions. Notably, many signals that were flexible and unassigned in (A) are not detected. This data is consistent with the MAS NMR spectra in which we were not able to assign 18 N- and C- terminal residues, as well as part of L1, T2 and T3, and the His_8 tag. The absence of peaks in assignment spectra indicates that some of these unassigned resonances correspond to residues that are highly flexible.

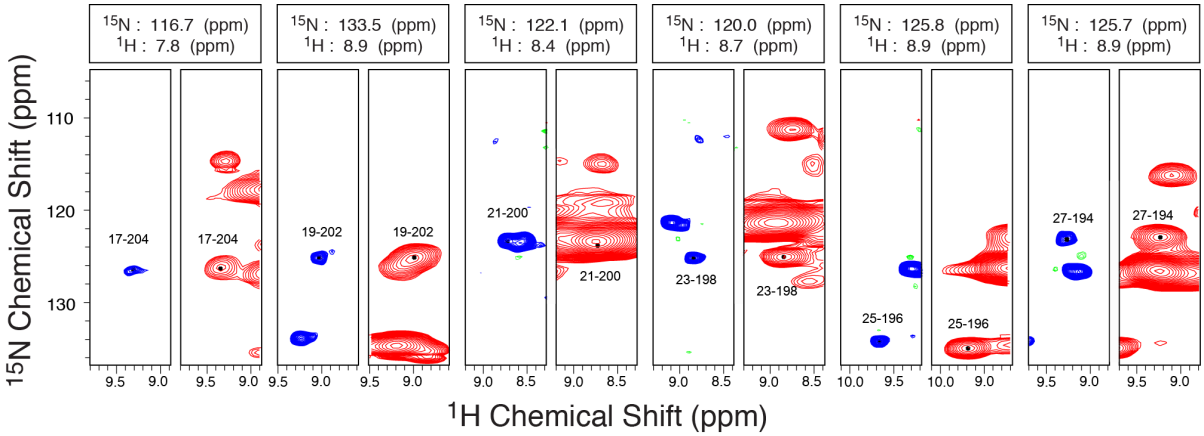

Figure S5. Inter-proton proximities. Selected planes from two 4D (H)NH(H)NH spectra (using RFDR for proton-proton mixing). In blue, the spectrum was recorded with high resolution, but lower sensitivity, by sampling the proton dimension to 4 ms. In red, the spectrum was recorded with shorter indirect proton evolution of 2 ms which resulted in higher sensitivity, but lower resolution. The first 2 planes (connecting residues 17-204) show an example where the peak was just above noise in the blue spectrum, and clearly found in the red spectrum. The third 2 planes (connecting residues 21-200) shows an example where the longer evolution times in the blue spectrum was necessary, and the peak is indistinguishable from the diagonal in the red spectrum. Both spectra were used in conjunction to construct a consistent set of nearly unambiguous contacts, and to build the initial model (see Fig. S6).

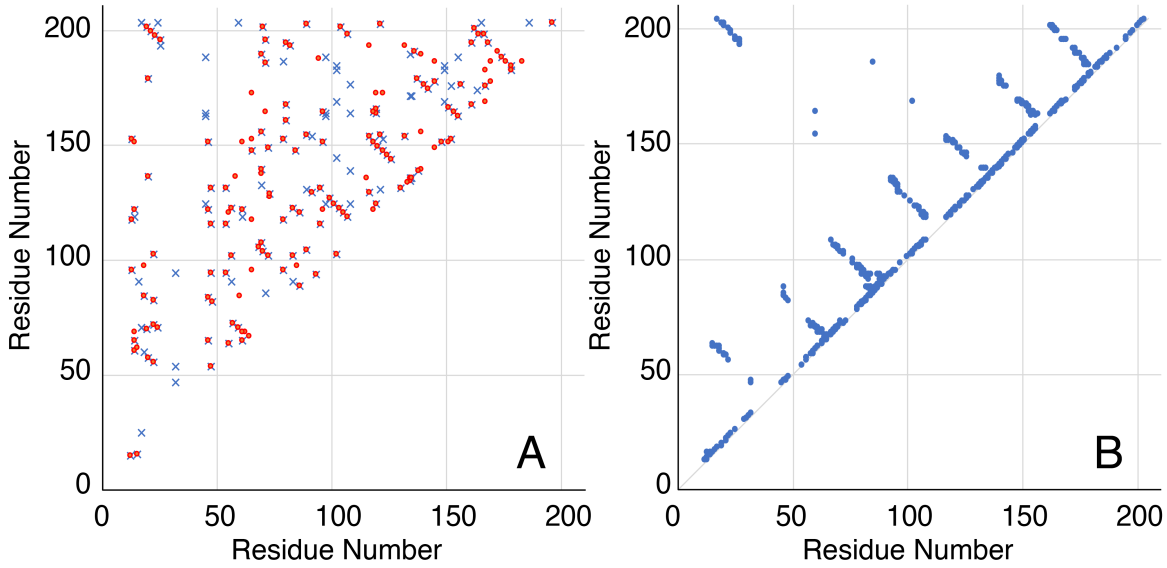

Figure S6. Proton-proton contact maps. In (A), automatically generated contacts from peaks picked from the (H)NH(H)NH spectra of Fig. S5. A threshold of 0.5 ppm (^{15}N) and 0.11 ppm (^{1}H) were used to generate all possible assignments. Contacts arising from one side of the spectrum's diagonal are shown in red, while those from the other are shown in blue. A clear pattern of antiparallel β-strands emerges, despite some degeneracy in the ^{1}H-^{15}N plane used to identify starting and ending signal. In (B), the contact map of the final structure is shown, after resolution of ambiguities using CYANA, and including contacts from all spectra. The additional restraint assignment possibilities in (A) arising from degenerate chemical shifts have been removed in (B).

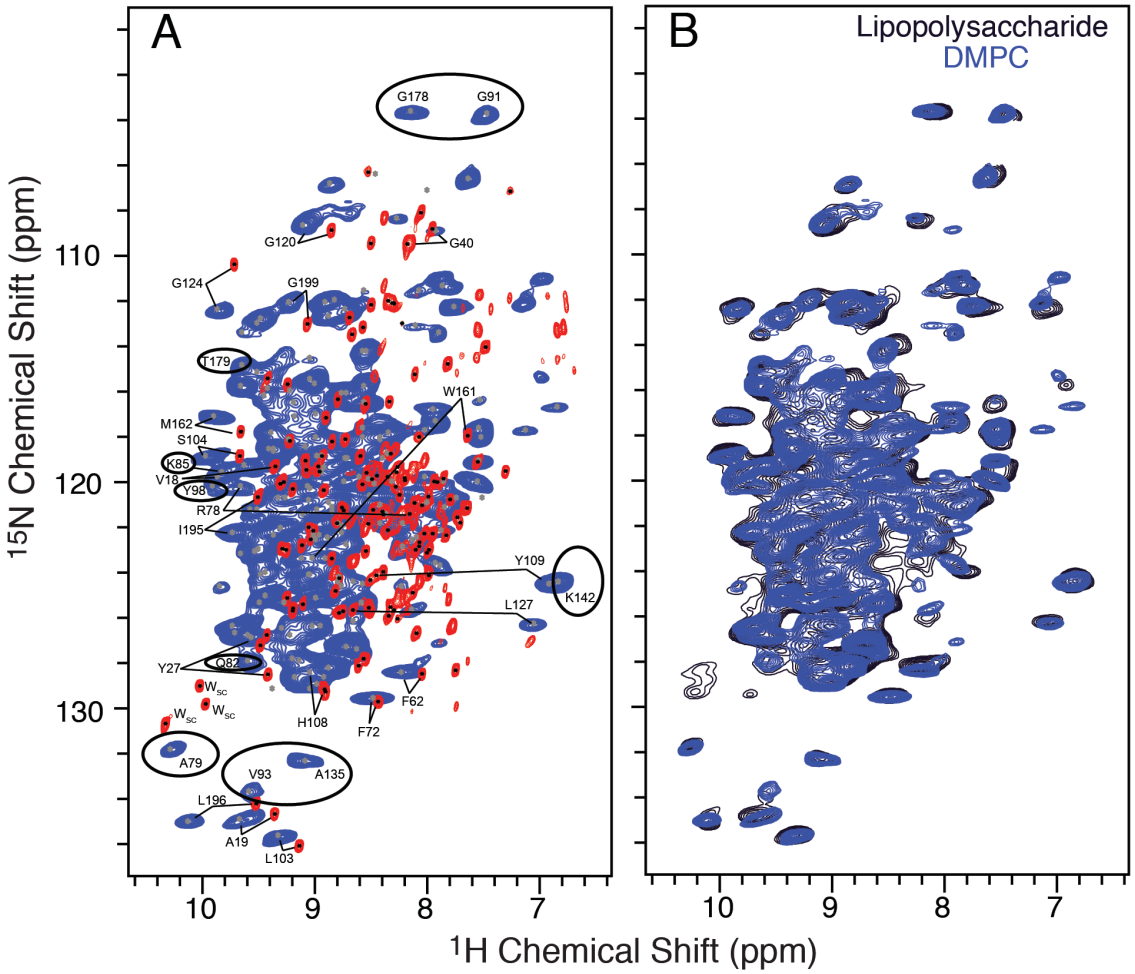

Figure S7. Solution and solid-state NMR spectra of AlkL. In A, the solution ^{15}N-^{1}H HSQC spectrum (red) is compared with the dipolar ^{15}N-^{1}H correlation acquired on the DMPC lipid bilayer sample (blue). Residues that were assigned in lipids, but could not be assigned in solution are encircled. Some of the residues outside the TM region displayed large differences in chemical shift, such as R78, Y109, L127, and W161, indicating the change from ordered to disordered. The remaining unassigned amide proton shifts in solution fall between 7.5 and 8.7 ppm, indicating a lack of β-sheet secondary structure. In B, the DMPC sample (blue) is compared with a sample reconstituted in 50% lipopolysaccharide (LPS) with a ratio of 1:0.5:0.5 AlkL:DMPC:LPS (w/w/w) (black). The spectra were contoured from 25% of the intensity of the G178 peak. The spectrum obtained in LPS, with only minor chemical shift changes, indicates that the structured extracellular loops are stable in the near native environment including lipopolysaccharides that are typically found on the outside of the asymmetric bacterial outer membrane. In the reconstituted sample, neither the AlkL, nor the LPS are oriented.

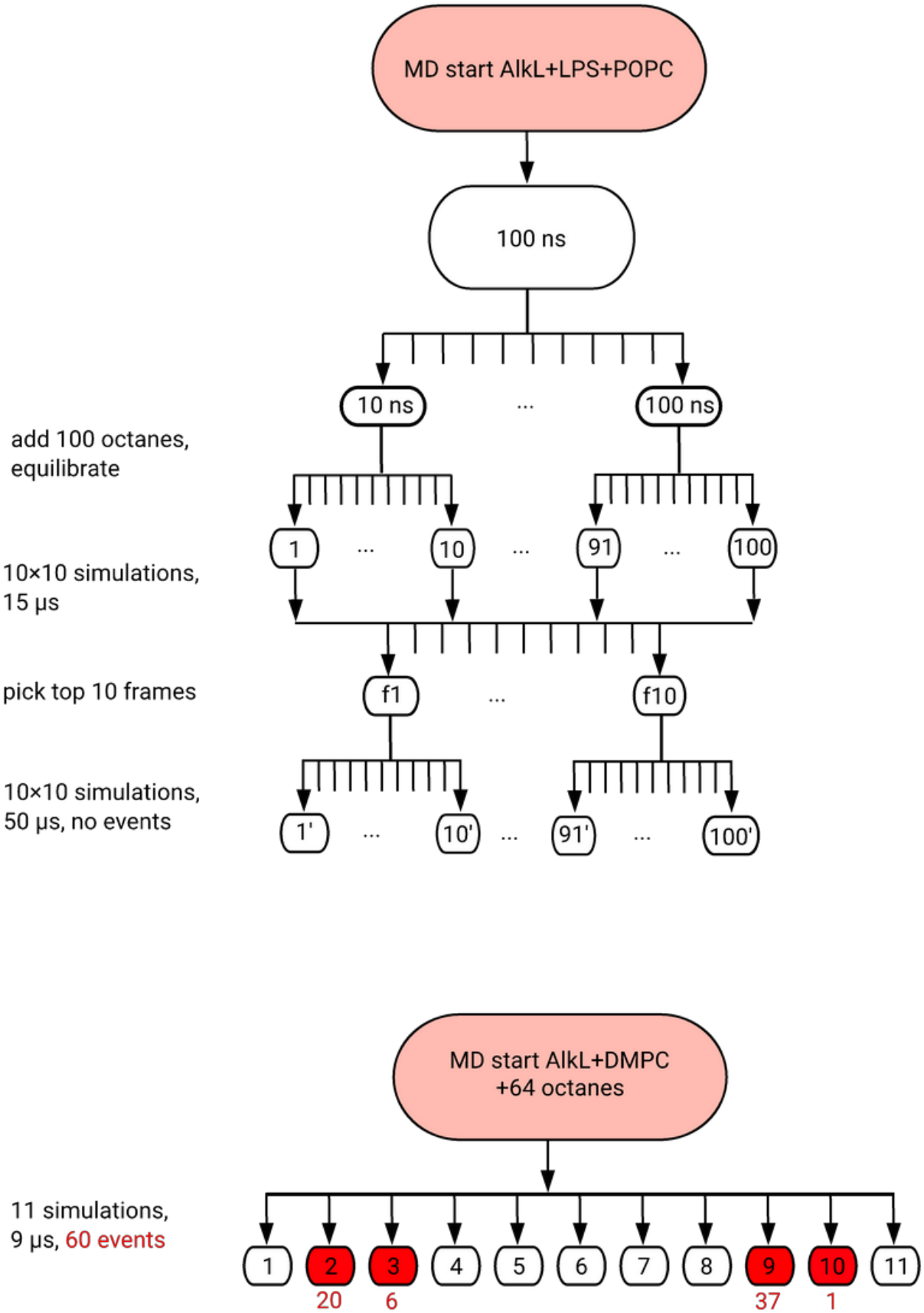

Figure S8. Simulation protocol for octane permeation through AlkL. Single numbers label individual simulation replicas. Simulations in which an octane molecule spontaneously permeated through the protein are indicated in red, along with the number of transit events observed.

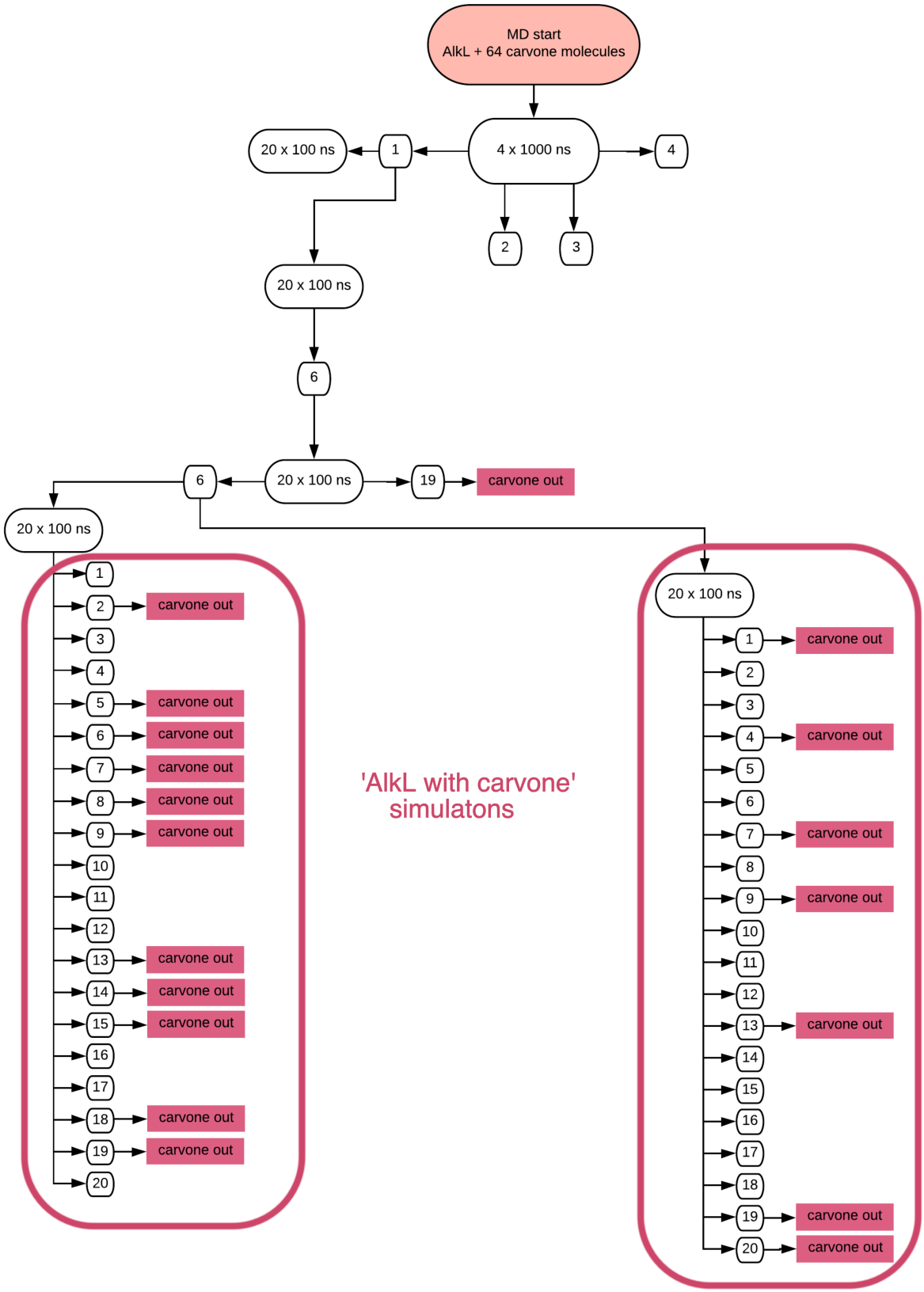

Figure S9. Simulation protocol for carvone permeation through AlkL. Single numbers label individual simulation replicas. Simulations in which a carvone molecule spontaneously permeated through the protein are labelled with boxes 'carvone out'. The 40 simulations referred to as 'AlkL with carvone' in the main text are enclosed within the rounded maroon boxes.

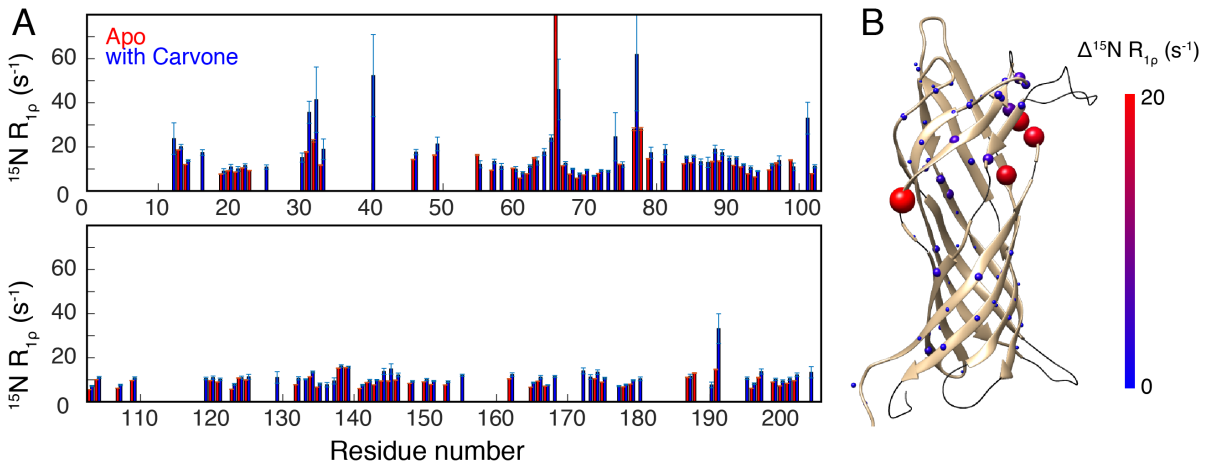

Figure S10. Dynamic parameter perturbations highlight weak binding sites of carvone. In A, transverse relaxation rates are shown for apo (red) and carvone saturated (blue) samples, as determined from (H)CONH spectra. In B, the difference in rates is shown on the structure.

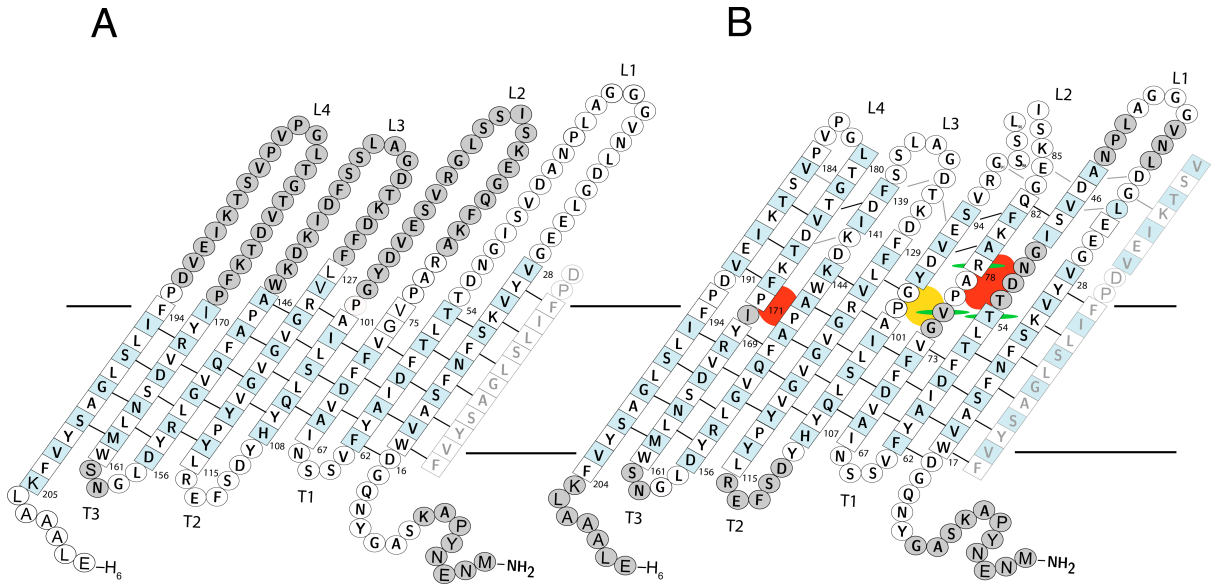

Figure S11. Topology map of AlkL as determined by NMR, both in detergent micelles (A) and in lipid bilayers (B). Assigned residues with chemical shifts consistent with β-sheet conformation are indicated in boxes, while other assigned residues are indicated with white circles. Unassigned residues are in grey circles. Blue residues point toward the interior. In lipids, a hydrophobic volume is formed in the extracellular barrel extension. The interior of the transmembrane β-barrel is packed densely with the side-chains of charged residues, while hydrophobic residues point out, as expected. Intracellular turns are numbered as T1-T3, and extracellular loops are numbered L1-L4. In both panels, in order to render the circular barrel topology, the last β-strand is repeated on the right-hand side and grayed out. The approximate position of the membrane is indicated by horizontal lines. The new and previous proposed exit sites are shown as red and yellow ovals, respectively, and packing interactions in OmpW crystals are indicated by green lines.

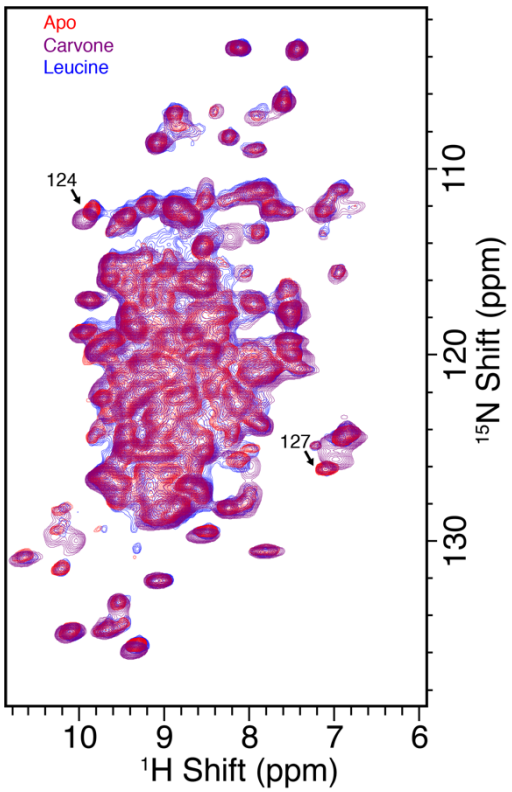

Figure S12. Chemical shift perturbations due to saturation with carvone (purple), which has about 7-8 mM solubility in water(31) and 1 mg/ml (8 mM) Leucine (blue). Shift changes of similar magnitude are observed with octane, which has a very low solubility in water (only about 60 nM according to the CDC NIOSH https://www.cdc.gov/niosh/npg/npgd0470.html. The shift changes due to carvone are evident in the 2D spectrum. For leucine, no shift changes are seen, consistent with the expectation that AlkL does not act as a channel for amino acids.

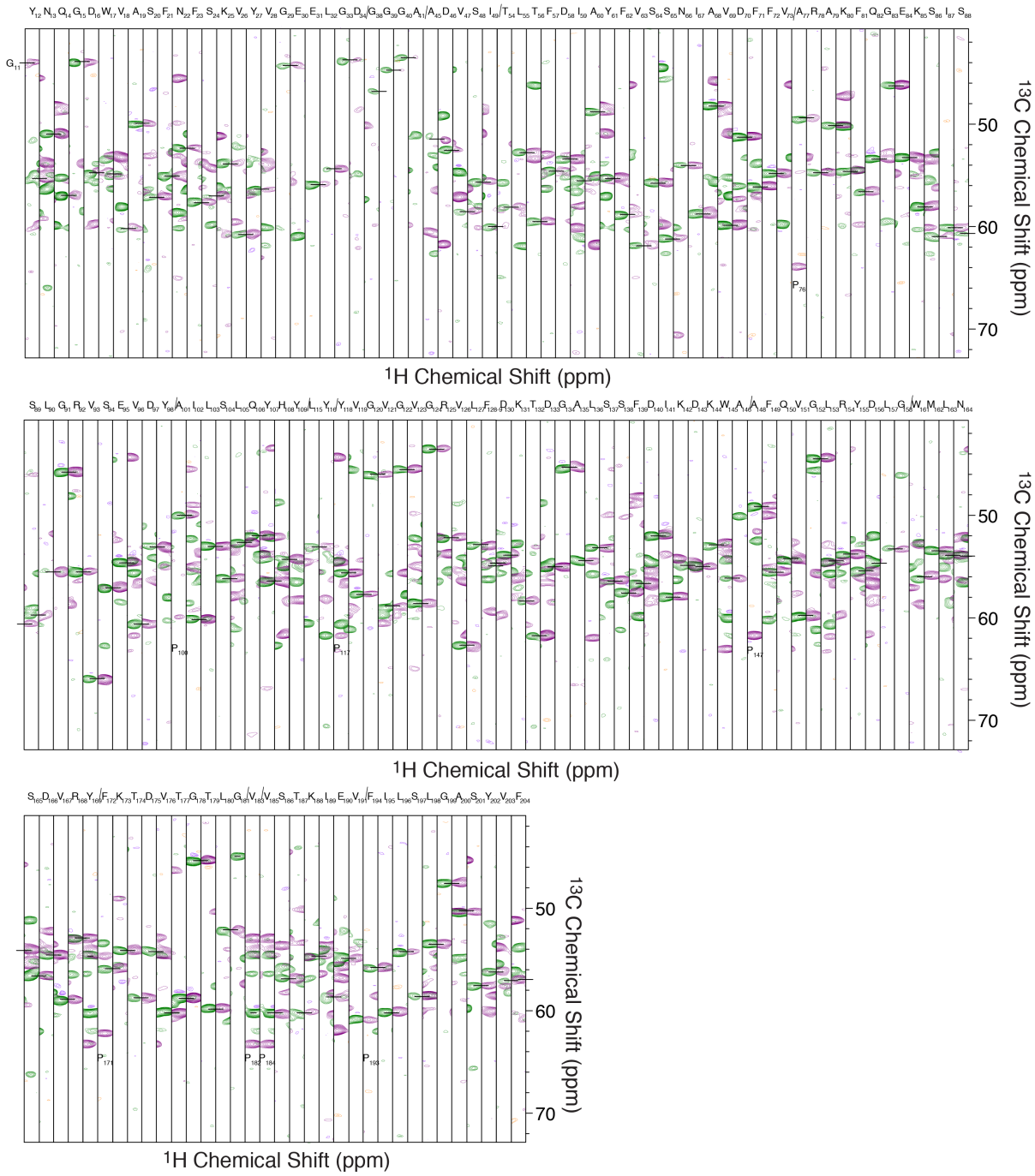

Figure S13. Backbone resonance assignment. Linking of sequential NH moieties in the (H)CANH (green) and (H)(CO)CA(CO)NH (purple) spectra of ^{2}H,^{13}C,^{15}N AlkL in lipid bilayers. Strips corresponding to each assigned NH group are shown. The sequence specific assignment is indicated above each strip, and a slash indicates where assignments are missing.

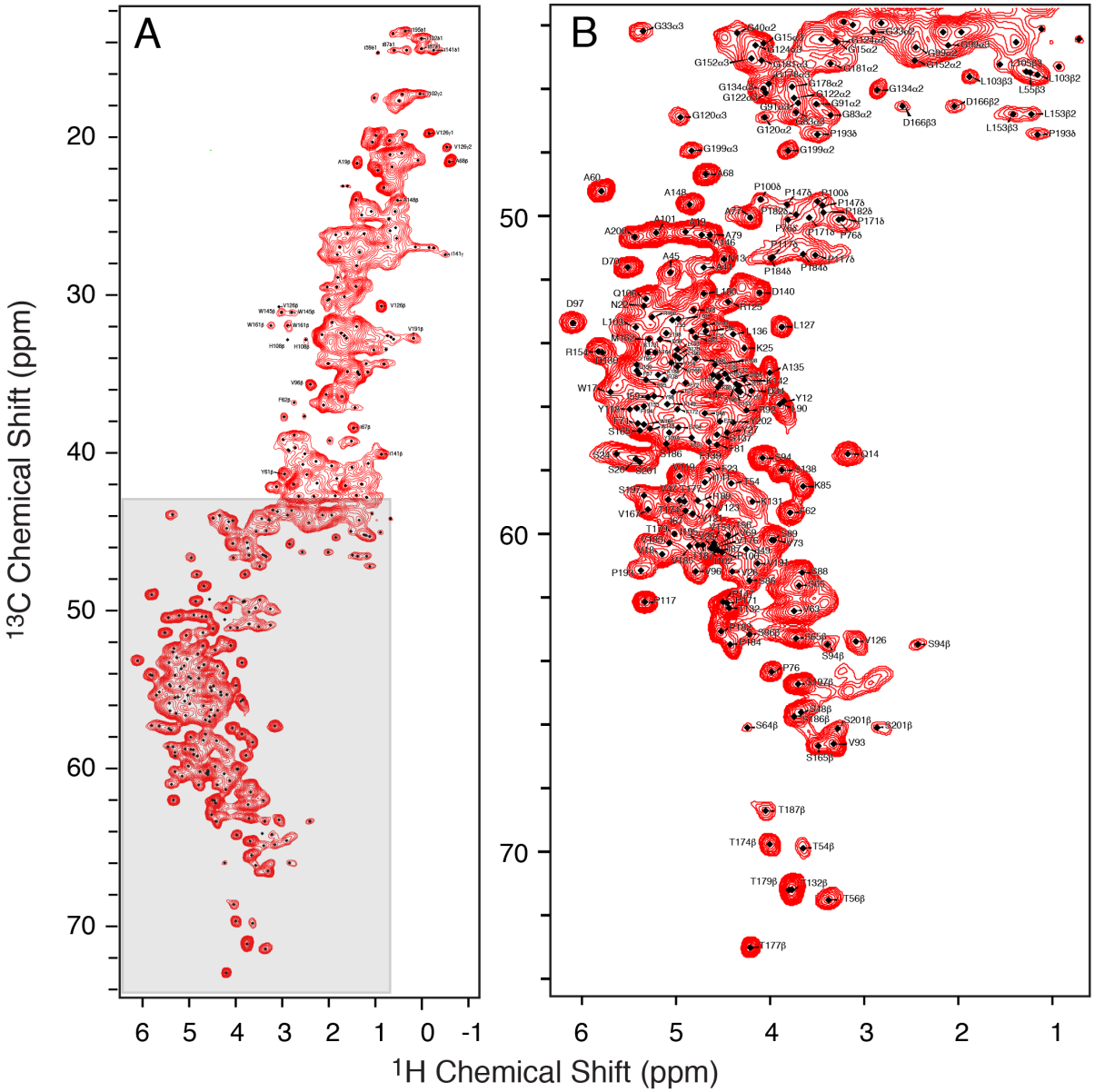

Figure S14. Solid-state NMR ^{1}H-^{13}C dipolar correlation spectrum recorded on lipid bilayer embedded U-^{13}C,^{15}N AlkL using 111 kHz magic-angle spinning. Assignments are shown for the C□-H□ region (right), as well as for selected isolated side-chain peaks (left).

SI Movie. The motion along the first (largest) eigenvector in a principal component analysis of MD snapshots with and without the molecule carvone. The motion shows that the difference without and with bound carvone is related to the opening of the newly identified site I for carvone permeation.

SI References

1. Schwarzer TS, Hermann M, Krishnan S, Simmel FC, & Castiglione K (2017) Preparative refolding of small monomeric outer membrane proteins. *Protein Expr. Purif.* 132:171-181.
2. Jain MG*, et al.* (2017) Selective (1)H-(1)H Distance Restraints in Fully Protonated Proteins by Very Fast Magic-Angle Spinning Solid-State NMR. *J. Phys. Chem. Lett.* 8:2399-2405.
3. Ritchie TK*, et al.* (2009) Chapter 11 - Reconstitution of membrane proteins in phospholipid bilayer nanodiscs. *Methods Enzymol.* 464:211-231.
4. Salzmann M, Wider G, Pervushin K, Senn H, & Wuthrich K (1999) TROSY-type triple-resonance experiments for sequential NMR assignments of large proteins. *J. Am. Chem. Soc.* 121:844-848.
5. Barbet-Massin E*, et al.* (2014) Rapid proton-detected NMR assignment for proteins with fast magic angle spinning. *J. Am. Chem. Soc.* 136:12489-12497.
6. Stanek J*, et al.* (2016) NMR Spectroscopic Assignment of Backbone and Side-Chain Protons in Fully Protonated Proteins: Microcrystals, Sedimented Assemblies, and Amyloid Fibrils. *Angew. Chem. Int. Ed. Engl.* 55:15504-15509.
7. Bennett AE, Ok JH, Griffin RG, & Vega S (1992) Chemical-Shift Correlation Spectroscopy in Rotating Solids - Radio Frequency-Driven Dipolar Recoupling and Longitudinal Exchange. *J. Chem. Phys.* 96:8624-8627.
8. Schmidt E & Guntert P (2012) A new algorithm for reliable and general NMR resonance assignment. *J. Am. Chem. Soc.* 134:12817-12829.
9. Lee W, Tonelli M, & Markley JL (2015) NMRFAM-SPARKY: enhanced software for biomolecular NMR spectroscopy. *Bioinformatics* 31:1325-1327.
10. Vranken WF*, et al.* (2005) The CCPN data model for NMR spectroscopy: development of a software pipeline. *Proteins* 59:687-696.
11. Shen Y & Bax A (2013) Protein backbone and sidechain torsion angles predicted from NMR chemical shifts using artificial neural networks. *J. Biomol. NMR* 56:227-241.
12. Güntert P & Buchner L (2015) Combined automated NOE assignment and structure calculation with CYANA. *J. Biomol. NMR* 62:453-471.
13. Pettersen EF*, et al.* (2004) UCSF Chimera--a visualization system for exploratory research and analysis. *J. Comput. Chem.* 25:1605-1612.
14. Lomize MA, Pogozheva ID, Joo H, Mosberg HI, & Lomize AL (2012) OPM database and PPM web server: resources for positioning of proteins in membranes. *Nucleic Acids Res.* 40:D370-376.
15. Jo S, Kim T, Iyer VG, & Im W (2008) CHARMM-GUI: a web-based graphical user interface for CHARMM. *J. Comput. Chem.* 29:1859-1865.
16. Olsson MH, Sondergaard CR, Rostkowski M, & Jensen JH (2011) PROPKA3: Consistent Treatment of Internal and Surface Residues in Empirical pKa Predictions. *J. Chem. Theory Comput.* 7:525-537.
17. Van Der Spoel D*, et al.* (2005) GROMACS: fast, flexible, and free. *J. Comput. Chem.* 26:1701-1718.
18. Huang J*, et al.* (2017) CHARMM36m: an improved force field for folded and intrinsically disordered proteins. *Nat. Methods* 14:71-73.
19. Klauda JB*, et al.* (2010) Update of the CHARMM all-atom additive force field for lipids: validation on six lipid types. *J Phys Chem B* 114:7830-7843.
20. Vanommeslaeghe K*, et al.* (2010) CHARMM general force field: A force field for drug-like molecules compatible with the CHARMM all-atom additive biological force fields. *J. Comput. Chem.* 31:671-690.
21. MacKerell AD*, et al.* (1998) All-atom empirical potential for molecular modeling and dynamics studies of proteins. *J. Phys. Chem. B* 102:3586-3616.
22. Beglov D & Roux B (1994) Finite Representation of an Infinite Bulk System - Solvent Boundary Potential for Computer-Simulations. *J. Chem. Phys.* 100:9050-9063.
23. Hess B, Bekker H, Berendsen HJC, & Fraaije JGEM (1997) LINCS: A linear constraint solver for molecular simulations. *J. Comput. Chem.* 18:1463-1472.
24. Darden T, York D, & Pedersen L (1993) Particle Mesh Ewald - an N.Log(N) Method for Ewald Sums in Large Systems. *J. Chem. Phys.* 98:10089-10092.
25. Hoover WG (1985) Canonical dynamics: Equilibrium phase-space distributions. *Phys. Rev. A Gen. Phys.* 31:1695-1697.

26. Nose S (1984) A Unified Formulation of the Constant Temperature Molecular-Dynamics Methods. *J. Chem. Phys.* 81:511-519.
27. Parrinello M & Rahman A (1981) Polymorphic Transitions in Single-Crystals - a New Molecular-Dynamics Method. *J. Appl. Phys.* 52:7182-7190.
28. Sehnal D*, et al.* (2013) MOLE 2.0: advanced approach for analysis of biomacromolecular channels. *J. Cheminform.* 5:39.
29. Mercadante D, Grater F, & Daday C (2018) CONAN: A Tool to Decode Dynamical Information from Molecular Interaction Maps. *Biophys. J.* 114:1267-1273.
30. Humphrey W, Dalke A, & Schulten K (1996) VMD: visual molecular dynamics. *J. Mol. Graph.* 14:33-38, 27-38.
31. Fichan I, Larroche C, & Gros JB (1999) Water solubility, vapor pressure, and activity coefficients of terpenes and terpenoids. *J. Chem. Eng. Data* 44:56-62.